



Chemical Deposition of Tin Nanoparticles on Highly Porous Carbon-Coated Graphite and Its Electrochemical Characterization as an Anode for Lithium Ion Batteries

Yunhwa Kim¹ · Gyungse Park³ · Jung-Chul An⁴ · Ho-Jung Sun¹ · Joongpyo Shim²

Received: 28 April 2021 / Revised: 26 June 2021 / Accepted: 8 July 2021 / Published online: 12 July 2021
© The Korean Institute of Electrical and Electronic Material Engineers 2021

Abstract

Sn nanoparticles deposited on highly porous carbon-coated graphite were prepared as anode materials in lithium-ion batteries. Graphite was coated with carbon layer by the carbonization of sucrose with silica nanopowders. The silica nanopowders were eliminated by a NaOH solution to prepare highly porous carbon-coated graphite and thereafter, it was treated with nitric acid to modify the surface of carbon layer. Finally, Sn nanoparticles were deposited on porous carbon-coated graphite by the chemical reduction of SnCl₂ at room temperature. The porous carbon layer formed by the incorporation of silica and the surface modification in acidic treatment increased the surface area of graphite and decreased the particle size of deposited Sn nanoparticles. The deposition of Sn nanoparticle enhanced initial capacity of anode in lithium-ion batteries. The porous carbon layer in Sn nanoparticle deposited on graphite led to increase higher initial capacity and longer cycling performance than bare graphite because Sn nanoparticles were strongly attached to porous carbon layer after long cycles.

Keywords Lithium-ion batteries · Sn nanoparticles · Porous carbon layer · Graphite · Anode

1 Introduction

Rechargeable Li-ion batteries have been greatly employed in portable electronic devices including cell phones, and laptop computers, with global demand, because they possess high energy densities and exhibit long cycling life. Recently, attempts have been made to expand their application to electric vehicles (EVs). The market-scale design of large rechargeable Li-ion batteries, for high-energy requirements,

such as in EVs, requires high energy and power density technologies [1, 2]. Rechargeable Li-ion batteries utilize carbon materials as anode, such as graphite, exhibiting stable cyclability and possessing a wide potential difference. However, the theoretical capacity of graphite (372 mAh/g) is limited by the formation of LiC₆. Therefore, it is necessary to develop a new anode material, which possesses a larger theoretical capacity for a high capacity Li-ion batteries [3].

Among the anode materials that can substitute graphite, there are several lithium storage metals, such as Si, Sn, Ge, Al, Sb, and In [4], Sn (with a high theoretical capacity of ~994 mAh/g), among them, has been widely studied as a representative of the lithium storage metals, with large theoretical capacities. However, mechanical stress occurred because of the severe volume change of ~300% during the insertion-desertion of lithium. Resultantly, the Sn particles in the electrode were cracked and pulverized during the continuous charging-discharging processes, thereby causing the Sn electrode to suffer a capacity decline and exhibit an unstable cycling performance. Thus, it is challenging to utilize them as an anode materials in Li-ion batteries [5, 6].

There are several important approaches to prevent the pulverization of the electrode. One of these is to utilize nano-sized Sn powders and the other is to utilize Sn-based

✉ Ho-Jung Sun
hjsun@kunsan.ac.kr

✉ Joongpyo Shim
jpshim@kunsan.ac.kr

¹ Department of Material Science and Engineering, Kunsan National University, Gunsan, Jeonbuk 54150, Korea

² Department of Nano and Chemical Engineering, Kunsan National University, Gunsan, Jeonbuk 54150, Korea

³ Department of Chemistry, Kunsan National University, Gunsan, Jeonbuk 54150, Korea

⁴ Energy Storage Materials Research Center, Research Institute of Industrial Science and Technology, Pohang, Gyeongbuk 37673, Korea

alloy composites (SnM, where M = Co, Mn, Fe, etc.). These composites can accommodate the volume change and the mechanical stress of Sn, during the insertion-desertion of lithium [7, 8]. Particularly, carbon materials are generally employed as matrix materials hosting metal particles because they experience a small volume changes during lithiation and delithiation, and also exhibit soft and flexible properties. Because of these characteristics, carbonaceous materials are known to improve the capacity of lithium storage metals, to withstand volume changes, when combined. Further, the composite can prevent the cracking and decomposition of the electrodes, by maintaining the mechanical stability (through the reduction of the mechanical stress) in the electrode. Sn and carbon composites may be prepared in various forms, such as Sn@C, Sn embedded in C, Sn/graphene composites, and Sn/carbon nanotubes [9–11].

Most of works for Sn-carbon composites have been conducted through mechanical or physical processes, such as mixing, sputtering, etc. This kinds of process could be limited to small scale of production. In this study, Sn nanoparticles were deposited on the porous carbon-coated graphite by a simple chemical reduction method, to minimize the stress by the volume change during charge–discharge process (Fig. 1). It is assumed that porous carbon layer decreased the size of Sn particles and improved the adhesion of the Sn nanoparticles to the graphite surface. Physical properties and electrochemical characterizations were investigated on the effect of porous carbon layer and Sn deposition.

2 Experimental

The porous carbon-coated graphite powders were prepared by following processes: sucrose ($C_{12}H_{22}O_{11}$, Aldrich), as a carbon precursor, was first dissolved in deionized (DI) water with ethanol, after which graphite powder ($< 20 \mu\text{m}$, Aldrich) and silica nano powders ($\sim 10 \text{ nm}$, JIOS) were added to the solution. Thereafter, this suspension was stirred at $60 \text{ }^\circ\text{C}$ to evaporate the water. Next, the completely dried powders were heated in a tube furnace, in an N_2 atmosphere,

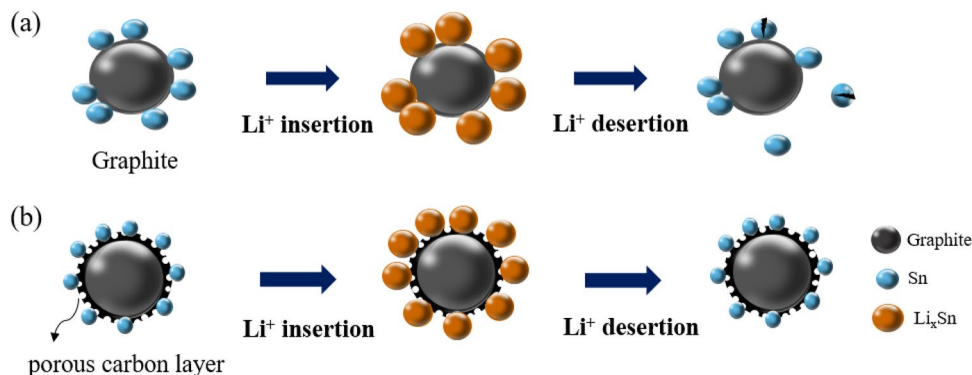
at $700 \text{ }^\circ\text{C}$ for 2 h. After the heat treatment, the powders were stirred in a 1 M NaOH solution for 24 h to remove the silica nanopowders. Finally, the obtained powder (named as pcG) were filtered and washed three times with DI water. Further, pcG was dispersed in a 1 M nitric acid solution and stirred for 6 h to modify the surface of pcG. The powders, with a modified surface, were filtered and washed for three times (named as pcG-NA).

Next, Sn nanoparticles (NPs) were deposited on the substrates (G, pcG, and pcG-NA) by a simple chemical reduction method. Therein, SnCl_2 and NaBH_4 were used as the Sn precursor and reducing agent, respectively [12]. The pcG or pcG-NA was added to 170 ml of 1 M SnCl_2 solution. Thereafter, 850 ml of 2 M NaBH_4 solution was added dropwise, into the SnCl_2 solution, at a rate of 1 drop/s with stirring. Resultantly, Sn NPs were deposited on the substrate, by the reduction of SnCl_2 . During this procedure, the N_2 gas was purged into the solution to prevent the oxidation of Sn NPs. After stirring, the suspension was filtered, washed by DI water, and dried, to obtain Sn deposited on substrates (named as Sn/G, Sn/pcG and Sn/pcG-NA).

A thermogravimetric analysis (TGA, SDT Q600, TA Instruments) was employed to measure the amount of coated carbon and deposited Sn on the graphite. The weight loss was observed by heating the sample up to $900 \text{ }^\circ\text{C}$ at the rate of $10 \text{ }^\circ\text{C}/\text{min}$ in the air atmosphere. The surface morphology and elemental analysis of the samples were observed by field-emission scanning electron microscopy (FE-SEM, SU8220, Hitachi), energy dispersive X-ray spectroscopy (EDS, HORIBA EX 250) and X-ray photoelectron spectroscopy (XPS, JEOL, JEM-ARM200F). The crystallinity of the samples was characterized by X-ray diffraction (XRD, EMPYRAN, Cu- $K\alpha$ radiation), in the range of 10° – 90° . The specific surface area of the samples was measured by the Brunauer–Emmett–Teller (BET, BELSORP-MAX, MicrotracBEL Corp) analysis, and the graphitization degree of G and pcG were determined by Raman spectroscopy (NT-MDT, NTEGRA).

The anode was prepared by using active materials (G, Sn/G, Sn/pcG and Sn/pcG-NA), Super-P (TIMCAL) as a

Fig. 1 Schematic diagrams for change of Sn particles during charge and discharge in **a** Sn NP on graphite (Sn/G) and **b** Sn NP on porous carbon-coated graphite (Sn/pcG)



conductive additive, and polyvinylidene fluoride (PVDF, Kynar 301F) as a binder. These materials were mixed in the ratio of 85:5:10. N-Methyl-2-pyrrolidone (NMP, JUNSEI) was added to make a slurry with proper viscosity. The uniformly mixed slurry was cast on a Cu foil with 200 μm thickness. The prepared electrode was dried at 60 $^{\circ}\text{C}$ for 12 h in an oven, and thereafter, it was vacuum-dried at 120 $^{\circ}\text{C}$ for 2 h.

CR2032 coin cells (Hoshen) were assembled in an Ar-filled glove box to measure the electrochemical properties. A Li foil (200 μm thick, Honjo Metal), 1 M LiPF_6 in ethylene carbonate/diethyl carbonate/ethyl methyl carbonate (EC/DEC/EMC, Soulbrain Co.), and a porous polypropylene membrane (Celgard 2500) were used as the counter electrode, electrolyte, and separator, respectively. Charge–discharge tests were conducted at room temperature at a voltage range of 0.01–2.0 V (vs. Li/Li^+) by a battery cycler (WBCS3000, WonAtech). The first and second cycles were conducted at the current density of 0.05C to understand the charging–discharging behaviors. Thereafter, the cells were tested at various C rates in the range of 0.2–5 C to investigate the rate capability. The cycling performance was measured during 100 cycles at 0.2 C. The C rate was calculated from the theoretical capacities of Sn and G.

3 Result and Discussion

The amounts of carbon coatings and Sn NPs in the samples were determined simply by TGA. When the samples were heat-treated in air, G and carbon were decomposed and the Sn particles changed to SnO_2 . As shown in Fig. 2a, G was completely decomposed around 650 $^{\circ}\text{C}$, resulting in weight loss. However, the combustion of pcG was occurred in two steps. The first step occurred at 450–600 $^{\circ}\text{C}$, and the second step started at ~ 600 $^{\circ}\text{C}$. This implies that the G substrate and porous carbon layer were decomposed at different temperatures because of the graphitic and amorphous carbons. Close to first step, ~ 10 wt% of the weight loss, which was induced by coated amorphous carbon on G, was calculated [13, 14].

For Sn/G, beyond 400 $^{\circ}\text{C}$, the weight was slightly increased according to the formation of SnO_2 . When the temperature exceeded 800 $^{\circ}\text{C}$, all carbon materials were decomposed and Sn was changed into an oxide. The amount of Sn on G could be calculated from the residues of the materials, and are assigned to SnO_2 . The TGA results confirmed that the Sn content of Sn/G, Sn/pcG, and Sn/pcG-NA were 36.6, 23.1, and 12.8 wt%, respectively.

XRD analysis was conducted to confirm the presence and crystal structure of the Sn particles. As shown in Fig. 2b, all the samples exhibited peaks at 26.5 $^{\circ}$, corresponding to [002] of graphite. Sn/G exhibited sharp peaks at 30.6, 32.0, 43.9, and 45.0 $^{\circ}$ associated with [200], [101], [220], and [211] of Sn, respectively, and Sn/pcG displayed tiny peaks, corresponding to Sn [15]. However, Sn/pcG-NA did not exhibit a peak related to Sn. The presence of Sn in Sn/pcG and Sn/pcG-NA were confirmed by different analytical tools.

Figure 3a shows the Raman spectra of G and pcG. The peaks in both G and pcG were observed at 1350 and 1580 cm^{-1} , and were assigned to sp^3 carbon (D band) and sp^2 carbon (G band), respectively [16]. Employing the areas of the D and G bands, the I_D/I_G ratio can be calculated. This is an index of the graphitization degree for carbon materials [17, 18]. The I_D/I_G ratio of G was 0.67 but that of pcG was 0.99. The I_D/I_G ratio of carbon materials is inversely proportional to the graphitization degree. Consequently, the graphitization degree of pcG was lower than that of G, implying that the porous carbon layer as an amorphous carbon was coated on the G particles. To obtain a uniform distribution of Sn NPs by increasing specific surface area, porous carbon layer was coated on the G substrate [19]. It was confirmed that the BET surface area of pcG was 109.11 m^2/g , which was 8.5 times higher than that of G (12.76 m^2/g), implying that porous carbon layer on graphite increased its surface area. The pores ~ 4 nm were sharply increased by carbon coating, as shown in Fig. 3b.

The morphology of materials was observed by SEM (Fig. 4). The surface of G was smooth, while that of pcG or pcG-NA was rough because of the porous carbon coating

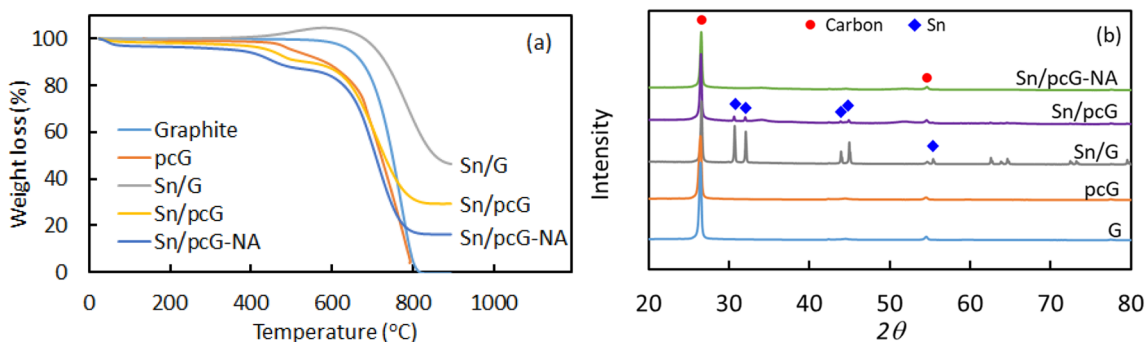


Fig. 2 a TGA curves under air atmosphere and b XRD patterns of graphite, pcG, Sn/G, Sn/pcG and Sn/pcG-NA

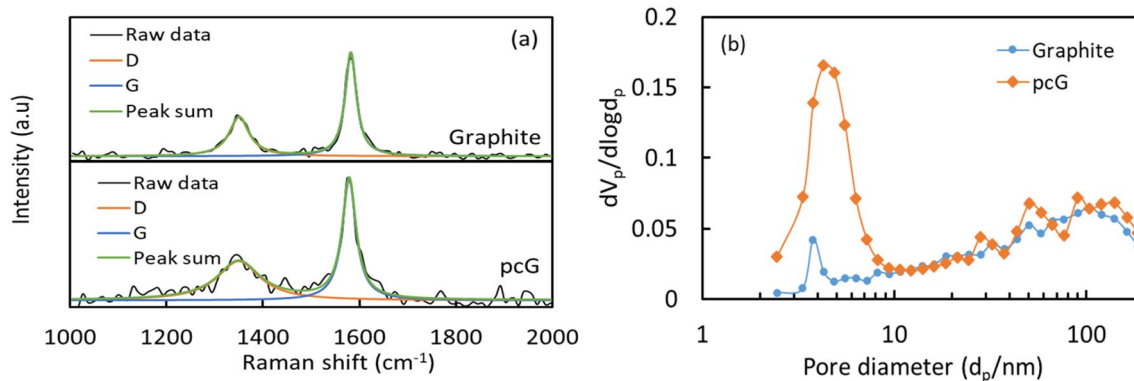


Fig. 3 **a** Raman spectra and **b** pore size distributions of graphite and pcG

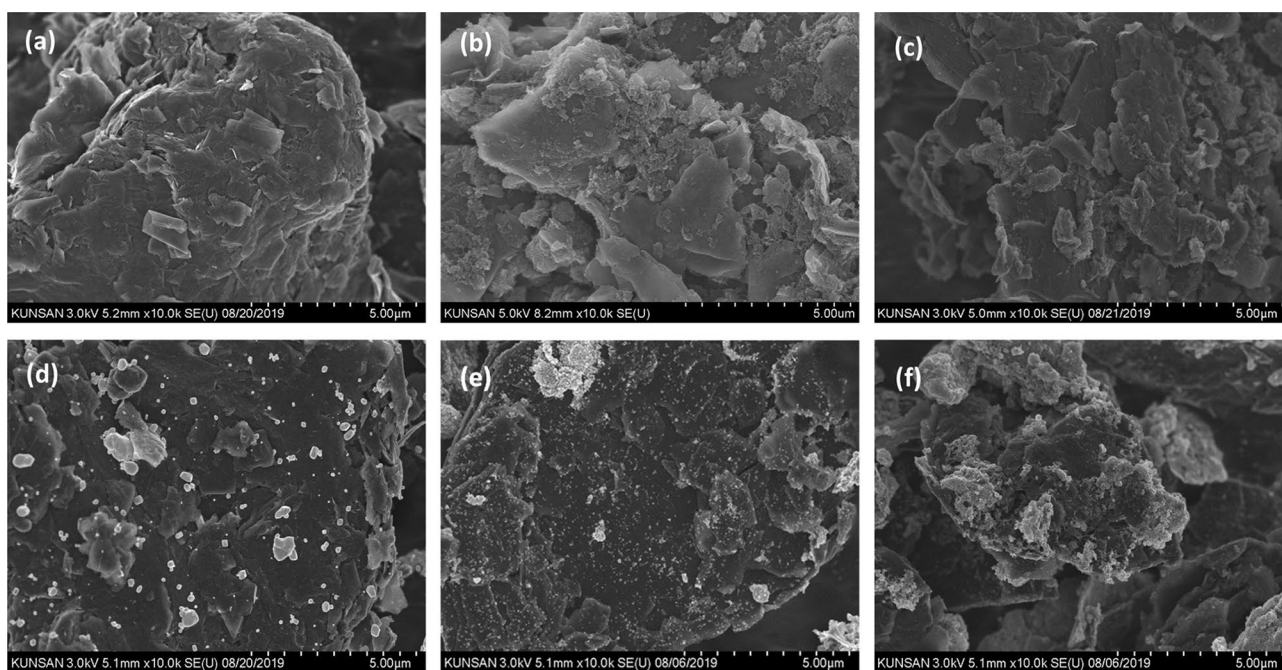


Fig. 4 SEM images of **a** graphite, **b** pcG, **c** pcG-NA, **d** Sn/G, **e** Sn/pcG, and **f** Sn/pcG-NA

(Fig. 4a–c). The SEM images of Sn/G are also shown in Fig. 4d–f. Sn/G in Fig. 4d clearly shows the presence of large-sized Sn particles on the surface. After carbon coating on graphite, the particle size of Sn significantly reduced, as clearly shown in Fig. 4e and f. Figure 5 shows the TEM images of Sn/G, Sn/pcG, and Sn/pcG-NA. Sn/G contained Sn particles with size of > 50 nm. The Sn particle sizes were reduced to ~20 nm in Sn/pcG, and < 10 nm in Sn/pcG-NA. The particle distributions were observed by EDS mapping of Sn (Fig. 5d–f). The Sn particles in Sn/pcG and Sn/pcG-NA achieved uniform distributions on pcG substrate. Further, utilizing the EDS mapping of Sn/pcG-NA in Fig. 5f, the presence of the Sn particle was confirmed, although the diffraction peaks of Sn were not found in Fig. 2.

Figure 6 shows the XPS results for Sn/G, Sn/pcG, and Sn/pcG-NA to identify the chemical status of Sn, C, and O, respectively. Figure 6b shows two peaks at 485.1 and 493.4 eV, which were assigned to the 3d_{5/2} and 3d_{3/2} of Sn, respectively. These two peaks corresponded to Sn, although Sn in Sn/pcG-NA was not detected in the XRD pattern [20]. In Fig. 6c, the peaks of C 1s were deconvoluted and assigned to the C–C (284.8 eV), C–OH (285.5 eV) and C=O (289.5 eV) groups. These assignments agree with those of previous results reported in the literature [21]. These deconvolutions suggested that the surfaces of carbon possessed oxygen-containing functional groups. Figure 6d shows the O 1s spectra, which were mostly assigned to the C=O (531.8 eV) and C–O (532.7 eV) signals, and exhibited a

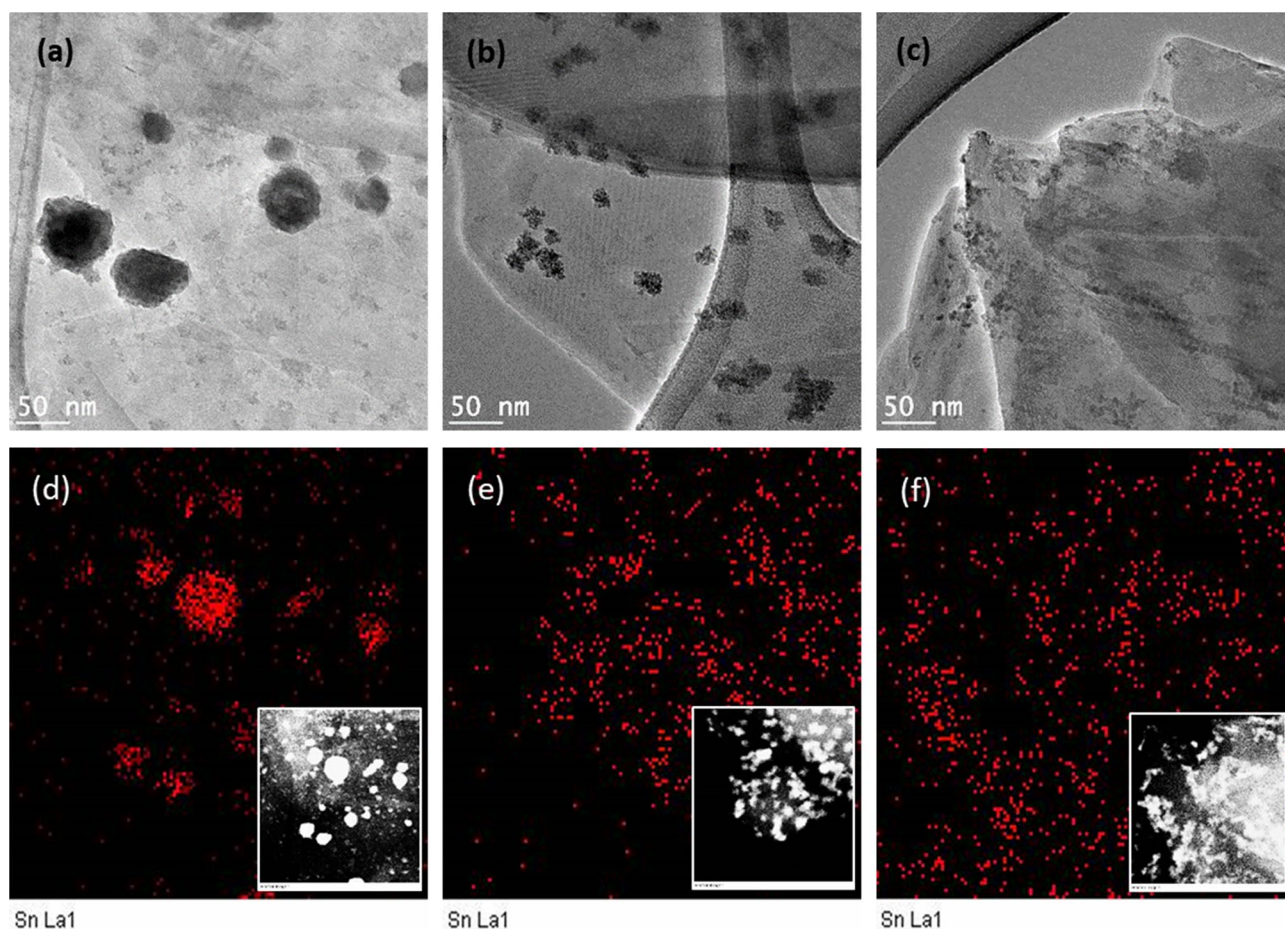


Fig. 5 TEM images and EDS mapping of Sn element for **a, d** Sn/G, **b, e** Sn/pcG and **c, f** Sn/pcg-NA

weak “absorbed oxygen” signal [22]. The peaks for O–Sn²⁺ and O–Sn⁴⁺ were not observed from the O 1s spectra [23], suggesting that Sn was deposited on the surface of the coated carbon layer. The detailed information and fitting of XPS for the three samples are shown in Table S1 and Fig. S1.

Figure 7a shows the first charge–discharge cycles of all the samples at 0.02C rate. The capacities of G in first and second cycles, which are slightly lower than theoretical capacity of graphite (372 mAh/g), were 329.6 and 327.4 mAh/g (Fig. S2(a)), respectively. G exhibited a coulombic efficiency of 89.5% at the first cycle but that was fully recovered at the second cycle. The capacities of pcG for first and second cycles, which are larger than capacity of G, were 352.5 and 426.4 mAh/g (Fig. S1(b)), respectively [24], explaining why the pores and defects of the amorphous carbon layer could accommodate Li ion. However, pcG exhibited a coulombic efficiency of 49.1% during the first cycle. The large irreversible capacity at first cycle was due to the side reaction of the electrolyte with porous carbon layer induced by increased surface area. The coulombic efficiency of pcG recovered to 89.5% at the second cycle.

The capacities of Sn/G, Sn/pcG, and Sn/pcG-NA were significantly increased because of the presence of the Sn particles. The capacities of Sn/G, Sn/pcG, and Sn/pcG-NA at the first cycle were 447.9, 517.1, and 529.6 mAh/g, which are 136, 157 and 161%, respectively, higher than that of G. This confirms that the Sn particles, as active materials on the G substrate, formed compounds with Li and increased their capacities.

The rate capability was measured at different discharging rate of 0.2–5C with 0.2C charging rate (Fig. S3). All the electrodes exhibited a tendency to decrease the discharge capacity with increasing rate. G maintained the capacity of 295.2 mAh/g at 5C, which was 95.7% of the capacity at 0.2C. The pcG exhibited good capacity retention with increasing rate and maintained a large capacity of 390.0 mAh/g at 5C. The capacity of Sn/G was rapidly decreased to 292.6 mAh/g at 5C, which represented an 80.1% reduction of the capacity at 0.2C. Conversely, the Sn-deposited materials (Sn/pcG and Sn/pcG-NA) exhibited capacities of 427.8 and 403.4 mAh/g at 5C, respectively. Additionally, the capacity retention of Sn/pcG-NA at 5C was 86.8% of the

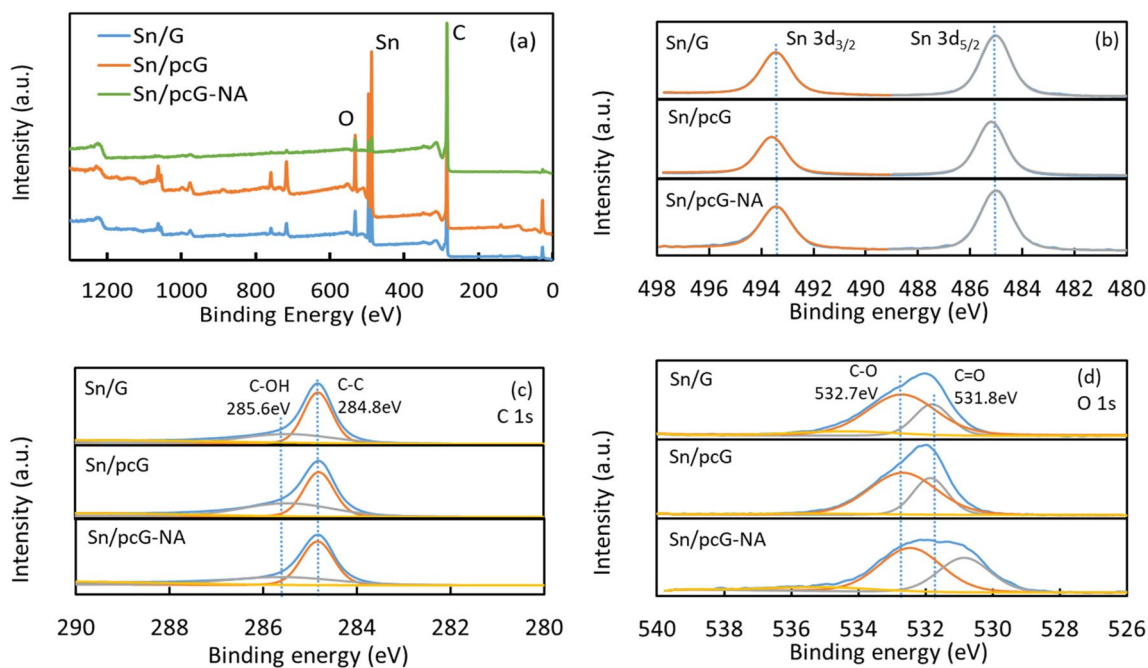


Fig. 6 XPS of Sn deposited samples, **a** all spectrum, **b** Sn 3d scan, **c** C 1s scan and **d** O 1s scan

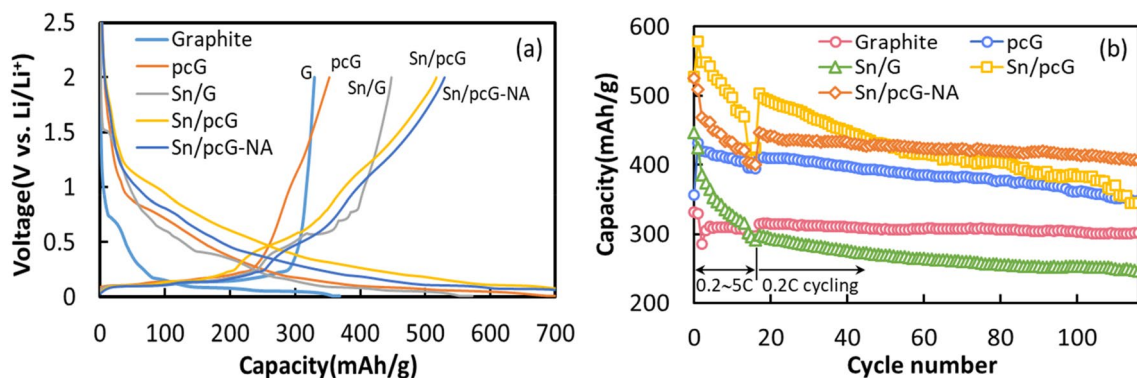


Fig. 7 **a** First charge and discharge cycles at 0.02C rate and **b** cycle performances at 0.2C rate for 120 cycles of graphite, pcG, Sn/G, Sn/pcG and Sn/pcG-NA

capacity at 0.2C. These results demonstrate that Sn particles exhibit better rate performances when they are deposited on a porous carbon layer than bare G substrate.

To evaluate the performance for continuous cycling, the cells were tested for 100 cycles at 0.2C after the rate capability test, as shown in Fig. 7b. The fading rate of G was 0.13 mAh/g cycle, exhibiting 302.3 mAh/g after 100 cycles. The pcG showed 347.7 mAh/g after 100 cycles and 0.60 mAh/g cycle, which was 4.6 times higher than bare G. Sn/G had the lowest capacity after 100 cycles (246.7 mAh/g). However, Sn/pcG and Sn/pcG-NA retained higher capacities than Sn/G after 100 cycles. Sn/pcG demonstrated a high capacity of 503.0 mAh/g at the beginning of the cycling but its

capacity dropped to 335.4 mAh/g after 100 cycles with a fading rate of 1.31 mAh/g cycle. Sn/pcG-NA showed 406.1 mAh/g after 100 cycles, which is the highest capacity among all samples, implying that Sn in composite accounted for 806 mAh/g-Sn of the capacity. The capacity fading rate of Sn/pcG-NA was dramatically decreased to 0.31 mAh/g cycle, which was half of that of pcG sample. Resultantly, when the Sn particles were deposited on the pcG substrate, it exhibited better cycling performance than when it was deposited on G. The summary of the cycling results and comparison with those in the literature are listed in Table S2.

Sn forms various intermetallic compounds, such as Li_2Sn_5 , LiSn , Li_5Sn_2 , $\text{Li}_{13}\text{Sn}_5$ and $\text{Li}_{22}\text{Sn}_5$, when it reacts

with Li-ion [25]. Figure 8a shows the dQ/dV plot for the first cycle of each sample. The dQ/dV plot demonstrated the insertion-desertion of Li ions into G and Sn. All the samples exhibited three large peaks below 0.3 V, which were assigned to the intercalation–deintercalation of Li ion in G, and small peaks in the range of 0.8–0.9 V due to electrolyte decomposition [26–28]. As shown in Fig. 8a, the dQ/dV plot of Sn/G for the first cycle notably exhibited several peaks, corresponding to the formation of Li-Sn intermetallic compounds. Sn/G exhibited the most distinct peaks for the reaction of Sn with Li-ions. Sn/pcG exhibited relatively small peaks and Sn/pcG-NA exhibited a broad peak. These peaks were assigned to the reaction between Li ion and Sn and proved that Sn reacts with Li to produce various alloys. The peaks at 0.63, 0.56, 0.42 and 0.38 V of the anodic sweep appeared and were assigned to the formations of Li_2Sn_5 , Li_5Sn_2 , Li_7Sn_2 , and $\text{Li}_{22}\text{Sn}_5$, respectively [29, 30]. Figure 8b and Fig. S4 show the dQ/dV plots of the final cycles (120th cycle) for Sn/G, Sn/pcG, and Sn/pcG-NA in the region for the formation of Lo-Sn compounds, and their comparison with those of the first cycles. The final cycle for Sn/G displayed no peak but Sn/pcG and Sn/pcG-NA exhibited broad peaks above 0.3 V, corresponding to Li insertion-desertion into Sn at the last cycle. In the case of Sn/G, it implies that Sn and Li could not react. In other words the Sn particles were electrochemically inactive by separating them from the G. Conversely, Sn in Sn/pcG and Sn/pcG-NA still reacted with Li ion at the last cycle, indicating that the Sn particles remained on porous carbon layer. The dQ/dV plots demonstrated that the Sn particles were strongly deposited on pcG and maintained the electrochemical activity after 120 cycles.

The benefit of the Sn deposited graphite composite anode are that the capacity could be increased to more than ~30%; the synthetic processes are simple, involving the chemical reduction of Sn compounds; and the electrode preparation procedures, including the component composition of electrode, do not require any change, as in the case of bare graphite.

4 Conclusions

In this study, Sn nanoparticles were successfully deposited on porous carbon-coated graphite substrates by a simple chemical reduction method at room temperature. The porous carbon on the graphite increases the surface area. The Sn nanoparticles on the porous carbon-coated substrate were smaller and more evenly distributed than those on bare substrate. Sn/G, Sn/pcG, and Sn/pcG-NA demonstrated 447.9, 517.1 and 529.6 mAh/g of capacities, respectively, which were higher than that of graphite, in the first cycle. They exhibited 427.8 and 403.4 mAh/g of capacities at a current density of 5C, respectively. Sn/pcG-NA demonstrated the most stable cycle performance and maintained 90.9% of its initial capacity for 100 cycles at a rate of 0.2C. The dQ/dV plots for the last cycle confirmed that the porous carbon coating prevented the separation of the deposited Sn particles. The pcG was able to successfully accommodate the stress due to the volume change of the Sn particles. Further, porous carbon coating improved the adhesion of the Sn particles, resulting in the successful deposition of Sn

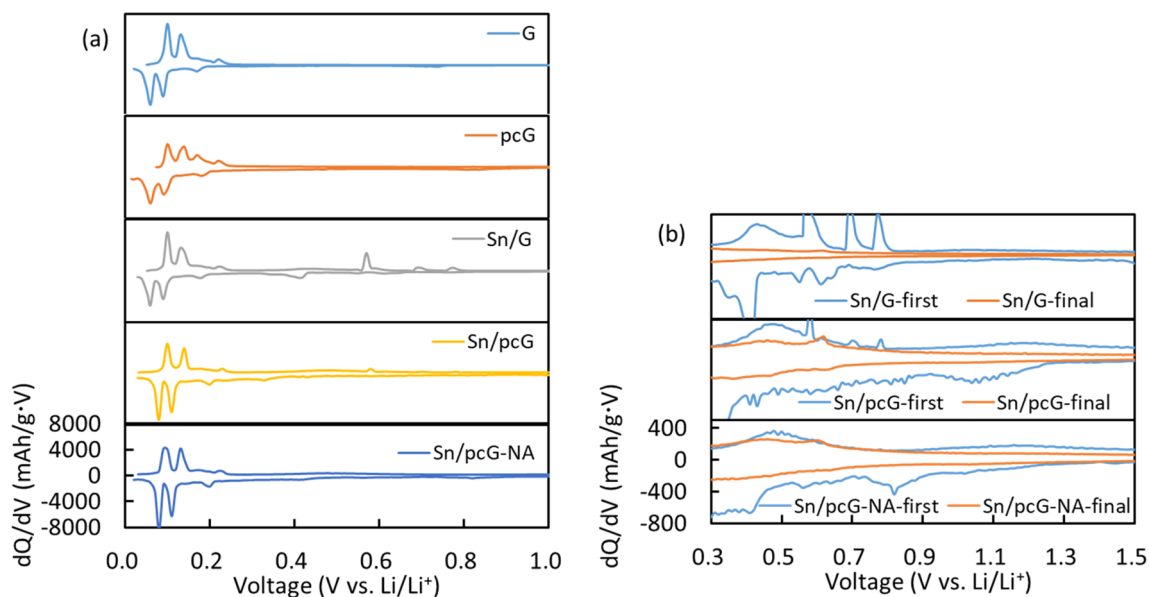


Fig. 8 dQ/dV plots of G, pcG, Sn/G, Sn/pcG, Sn/pcG-NA for **a** first cycle and **b** final cycle after 120 cycles

on graphite, in which the deposited Sn particles exhibited good rate performance and stable capacity retention during cycling.

Supplementary Information The online version contains supplementary material available at <https://doi.org/10.1007/s42341-021-00352-x>.

Acknowledgements This work was supported by the National Research Foundation of Korea Grant funded by the Korean Government (MEST) (2017-R1D1A3B03032610). Also, this work was supported by research fund of Kunsan National University for faculty member in the year 2020.

References

- N. Nitta, G. Yushin, High-capacity anode materials for lithium-ion batteries: choice of elements and structures for active particles. *Part. Part. Syst. Charact.* **31**, 317–336 (2014). <https://doi.org/10.1002/ppsc.201300231>
- J.L. Tirado, Inorganic materials for the negative electrode of lithium-ion batteries: state-of-the-art and future prospects. *Mater. Sci. Eng. R Rep.* **40**, 103–136 (2003). [https://doi.org/10.1016/S0927-796X\(02\)00125-0](https://doi.org/10.1016/S0927-796X(02)00125-0)
- T.-R. Kim, J.-Y. Wu, Q.-L. Hu, M.-S. Kim, Electrochemical performance of carbon/silicon composite as anode materials for high capacity lithium ion secondary battery. *Carbon Lett.* **8**, 335–339 (2007). <https://doi.org/10.5714/cl.2007.8.4.335>
- F. Nobili, M. Mancini, P.E. Stallworth, F. Croce, S.G. Greenbaum, R. Marassi, Tin-coated graphite electrodes as composite anodes for Li-ion batteries. Effects of tin coatings thickness toward intercalation behavior. *J. Power Sources* **198**, 243–250 (2012). <https://doi.org/10.1016/j.jpowsour.2011.09.075>
- A.R. Kamali, D.J. Fray, Tin-based materials as advanced anode materials for lithium ion batteries: a review. *Rev. Adv. Mater. Sci.* **27**, 14–24 (2011)
- X. Zhou, J. Bao, Z. Dai, Y.G. Guo, Tin nanoparticles impregnated in nitrogen-doped graphene for lithium-ion battery anodes. *J. Phys. Chem. C* **117**, 25367–25373 (2013). <https://doi.org/10.1021/jp409668m>
- X. Li, Y. Zhong, M. Cai, M.P. Balogh, D. Wang, Y. Zhang, R. Li, X. Sun, Tin-alloy heterostructures encapsulated in amorphous carbon nanotubes as hybrid anodes in rechargeable lithium ion batteries. *Electrochim. Acta.* **89**, 387–393 (2013). <https://doi.org/10.1016/j.electacta.2012.11.097>
- X. Huang, S. Cui, J. Chang, P.B. Hallac, C.R. Fell, Y. Luo, B. Metz, J. Jiang, P.T. Hurley, J. Chen, A hierarchical tin/carbon composite as an anode for lithium-ion batteries with a long cycle life. *Angew. Chem.* **127**, 1510–1513 (2015). <https://doi.org/10.1002/ange.201409530>
- F. Nobili, I. Meschini, M. Mancini, R. Tossici, R. Marassi, F. Croce, High-performance sn@carbon nanocomposite anode for lithium-ion batteries: lithium storage processes characterization and low-temperature behavior. *Electrochim. Acta.* **107**, 85–92 (2013). <https://doi.org/10.1016/j.electacta.2013.05.150>
- H. Wang, P. Gao, S. Lu, H. Liu, G. Yang, J. Pinto, X. Jiang, The effect of tin content to the morphology of Sn/carbon nanofiber and the electrochemical performance as anode material for lithium batteries. *Electrochim. Acta.* **58**, 44–51 (2011). <https://doi.org/10.1016/j.electacta.2011.08.075>
- J.L. Tirado, R. Santamaría, G.F. Ortiz, R. Menéndez, P. Lavela, J.M. Jiménez-Mateos, F.J. GómezGarcía, A. Concheso, R. Alcántara, Tin-carbon composites as anodic material in Li-ion batteries obtained by coprolysis of petroleum vacuum residue and SnO₂. *Carbon N. Y.* **45**, 1396–1409 (2007). <https://doi.org/10.1016/j.carbon.2007.03.041>
- N.A. Smith, N. Sekido, J.H. Perepezko, A.B. Ellis, W.C. Crone, Synthesis of dual phase bronze alloys from elemental nanoparticle constituents. *Scr. Mater.* **51**, 423–426 (2004). <https://doi.org/10.1016/j.scriptamat.2004.05.004>
- J. Lee, S. Won, J. Shim, G. Park, H.J. Sun, H.K. Lee, Electrochemical characteristics of silicon-carbon composite anodes for lithium rechargeable batteries. *Trans. Electr. Electron. Mater.* **15**, 193–197 (2014). <https://doi.org/10.4313/TEEM.2014.15.4.193>
- S. Osswald, G. Yushin, V. Mochalin, S.O. Kucheyev, Y. Gogotsi, Control of sp²/sp³ carbon ratio and surface chemistry of nano-diamond powders by selective oxidation in air. *J. Am. Chem. Soc.* **128**, 11635–11642 (2006). <https://doi.org/10.1021/ja063303n>
- Á. Caballero, J. Morales, L. Sánchez, Tin nanoparticles formed in the presence of cellulose fibers exhibit excellent electrochemical performance as anode materials in lithium-ion batteries. *Electrochim. Solid-State Lett.* **8**, 464–466 (2005). <https://doi.org/10.1149/1.1993388>
- S. Reich, C. Thomsen, Raman spectroscopy of graphite. *Philos. Trans. R. Soc. A Math. Phys. Eng. Sci.* **362**, 2271–2288 (2004). <https://doi.org/10.1098/rsta.2004.1454>
- K. Kim, K.J. Lopez, H.J. Sun, J.C. An, G. Park, J. Shim, Electrochemical performance of bifunctional Co/graphitic carbon catalysts prepared from metal-organic frameworks for oxygen reduction and evolution reactions in alkaline solution. *J. Appl. Electrochem.* **48**, 1231–1241 (2018). <https://doi.org/10.1007/s10800-018-1245-8>
- J. Schwan, S. Ulrich, V. Batori, H. Ehrhardt, S.R.P. Silva, Raman spectroscopy on amorphous carbon films. *J. Appl. Phys.* **80**, 440–447 (1996). <https://doi.org/10.1063/1.362745>
- P. Schneider, Adsorption isotherms of microporous-mesoporous solids revisited. *Appl. Catal. A Gen.* **129**, 157–165 (1995). [https://doi.org/10.1016/0926-860X\(95\)00110-7](https://doi.org/10.1016/0926-860X(95)00110-7)
- D.A. Zatsepin, A.F. Zatssepin, D.W. Boukhvalov, E.Z. Kurmaev, N.V. Gavrilov, Sn-loss effect in a Sn-implanted a-SiO₂ host-matrix after thermal annealing: a combined XPS, PL, and DFT study. *Appl. Surf. Sci.* **367**, 320–326 (2016). <https://doi.org/10.1016/j.apsusc.2016.01.126>
- M. Yi, Z. Shen, X. Zhang, S. Ma, Achieving concentrated graphene dispersions in water/acetone mixtures by the strategy of tailoring Hansen solubility parameters. *J. Phys. D Appl. Phys.* (2013). <https://doi.org/10.1088/0022-3727/46/2/025301>
- G. Wang, C. Feng, Electrochemical polymerization of hydroquinone on graphite felt as a pseudocapacitive material for application in a microbial fuel cell. *Polymers (Basel)* (2017). <https://doi.org/10.3390/polym9060220>
- Y. Yang, J. Liu, C. Li, L. Fu, W. Huang, Z. Li, Fabrication of pompon-like and flower-like SnO microspheres comprised of layered nanoflakes by anodic electrocrystallization. *Electrochim. Acta.* **72**, 94–100 (2012). <https://doi.org/10.1016/j.electacta.2012.04.029>
- L. Fransson, T. Eriksson, K. Edström, T. Gustafsson, J.O. Thomas, Influence of carbon black and binder on Li-ion batteries. *J. Power Sources* **101**, 1–9 (2001). [https://doi.org/10.1016/S0378-7753\(01\)00481-5](https://doi.org/10.1016/S0378-7753(01)00481-5)
- M. Winter, J.O. Besenhard, Electrochemical lithiation of tin and tin-based intermetallics and composites. *Electrochim. Acta.* **45**, 31–50 (1999). [https://doi.org/10.1016/S0013-4686\(99\)00191-7](https://doi.org/10.1016/S0013-4686(99)00191-7)
- J. Shim, K.A. Striebel, The dependence of natural graphite anode performance on electrode density. *J. Power Sources* **130**, 247–253 (2004)
- H. Nozaki, K. Nagaoka, K. Hoshi, N. Ohta, M. Inagaki, Carbon-coated graphite for anode of lithium ion rechargeable batteries: carbon coating conditions and precursors. *J. Power Sources* **194**, 486–493 (2009). <https://doi.org/10.1016/j.jpowsour.2009.05.040>

28. T. Ohzuku, Y. Iwakoshi, K. Sawai, Formation of lithium-graphite intercalation compounds in nonaqueous electrolytes and their application as a negative electrode for a lithium ion (shuttlecock) cell. *J. Electrochem. Soc.* **140**, 2490–2498 (1993). <https://doi.org/10.1002/chin.199351008>
29. R.A. Huggins, Materials science principles related to alloys of potential use in rechargeable lithium cells. *J. Power Sources* **26**, 109–120 (1989). [https://doi.org/10.1016/0378-7753\(89\)80020-5](https://doi.org/10.1016/0378-7753(89)80020-5)
30. J. Wang, I.D. Raistrick, R.A. Huggins, Behavior of some binary lithium alloys as negative electrodes in organic solvent based electrolytes. *J. Electrochem. Soc.* **133**, 457–460 (1986). <https://doi.org/10.1149/1.2108601>

Publisher's Note Springer Nature remains neutral with regard to jurisdictional claims in published maps and institutional affiliations.